Available online at www.sciencedirect.com
SCIENCE DIRECT®

Journal of the European Ceramic Society 24 (2004) 2959–2968

www.elsevier.com/locate/jeurceramsoc

Sintering behavior of partially crystallized barium titanate monolithic xerogels with different nano-crystalline structure

Jung-Hee Cho[a,*], Makoto Kuwabara[b]

[a]Department of Ceramic Engineering, Kangnung National University, 123 Jibyeon, Kangnung, Gangwon 201-702, South Korea
[b]Department of Materials Science, The University of Tokyo, 7-3-1 Hongo, Tokyo 113-8656, Japan

Received 22 July 2003; received in revised form 17 October 2003; accepted 25 October 2003

Abstract

The densification behavior of partially crystallized barium titanate ($BaTiO_3$) monolithic xerogels prepared by a high concentration sol-gel method with different degree of hydrolysis was examined as a function of sintering temperature. The structural evolution of the xerogels during thermal treatment has been monitored by nitrogen adsorption/desorption porosimetry, XRD, TG/DTA, TEM, and SEM measurements. Sintering behavior of the xerogels can be significantly influenced by their initial microstructure that was affected by the content of water used for hydrolysis. Density change with sintering temperature was different between xerogels with different degrees of hydrolysis. Hydrolysis water content is H_2O/Ba molar ratio, denoted as r_w. Xerogels with $r_w = 5.0$, having a lower porosity and smaller pore size with less agglomerated particles, were sintered to form ceramics with a relative density of about 97% at a temperature of 1100 °C, whereas this was only 83% for xerogels with $r_w = 5.7$ having relatively larger pore volume and pore size. The average pore size of the xerogels increased with increasing sintering temperature up to 700 °C. For temperatures over 700 °C, it continued to increase for xerogels with $r_w = 5.7$, but it fell for xerogels with $r_w = 5.0$ due to rapid densification. Microstructural changes of the xerogels are discussed as a function of heat treatment temperature.

Keywords: $BaTiO_3$; Microstructure-final; Nano-crystallites; Sintering; Sol-gel processes

1. Introduction

Barium titanate ($BaTiO_3$) is a well-known perovskite type ferroelectric material widely used in the electronic ceramics industry, due to its high dielectric constant (>1000) at room temperature; it will continue to be used in the manufacture of multilayer ceramic capacitors (MLCs), positive temperature coefficient (PTC) thermistors, dynamic random access memory (DRAM), and electro-optic devices in the 21st century.[1–5] There have been many investigations attempting to fabricate dense $BaTiO_3$ ceramics using the sol-gel technique.[6–9] Sol-gel processes ensure a homogeneous mixing of all metal cations at a molecular level, and facilitates crystallization at relatively low temperatures. Phule et al.[7] prepared dense $BaTiO_3$ ceramics (92–96% of the theoretical density) sintered at 1350 °C without using any sintering additives. They used sol-precipitated powders calcined at 950–1000 °C. Chaput et al.[8] obtained highly dense $BaTiO_3$ ceramics (97% of the theoretical density) with fine-grained uniform microstructure (1 μm) by sintering at low temperature without prior calcination. They used nano-sized pure barium titanate powders with cubic perovskite structure made by an alkoxide-hydroxide route. Most of the investigations placed their aim mainly on the preparation of monodispersed powders with high purity and high sinterability. On the other hand, there have been few studies dealing with powderless processing to obtain dense $BaTiO_3$ ceramics from monolithic barium titanate gels, because such monolithic gels show unfavorable sintering behavior due to their inherent large porosity.[10] Recently, Shimooka et al.[11–13] succeeded in synthesizing partially crystallized $BaTiO_3$ monolithic xerogels with high density and high sinterability using high concentration metal alkoxide solutions. However, the densification mechanism of the xerogels has not been fully understood yet.

In our previous paper,[14] we have shown that the microstructure of $BaTiO_3$ xerogels can be significantly

* Corresponding author.
E-mail address: twocho@empal.com (J.-H. Cho).

0955-2219/$ - see front matter © 2003 Elsevier Ltd. All rights reserved.
doi:10.1016/j.jeurceramsoc.2003.10.043

influenced by hydrolysis water content. The precipitated crystallite sizes and contents in the amorphous gel network decreased with decreasing hydrolysis water content. In the present paper, we examine change of the densification behavior of the xerogels prepared with different amounts of water for hydrolysis. These results will enable dense $BaTiO_3$ ceramics to be obtained from partially crystallized monolithic xerogels prepared by high concentration sol-gel method.

2. Experimental procedures

Optically clear and partially crystallized $BaTiO_3$ monolithic xerogels were prepared by hydrolysis of high concentration precursor solutions (1.1 mol/l) of metal alkoxides with water vapor to have hydrolysis water contents of 5.0 and 5.7, as reported previously for our work.[14] High concentration of Ba,Ti alkoxide precursor solutions (1.1 mol/l, 6 ml batch) were prepared by dissolving equimolar amounts of barium ethoxide ($Ba(OCH_2CH_3)_2$, High Purity Chemicals Laboratory, Osaka, Japan; purity >99%) and titanium isopropoxide ($Ti(OCH(CH_3)_2)_4$, High Purity Chemicals Laboratory, Osaka, Japan; purity >99%) in a mixed solvent of dehydrated methanol (CH_3OH) and 2-methoxyethanol ($CH_3OC_2H_4OH$) with a ratio of 60/40 in volume at room temperature with stirring for 48 h. The synthesis process of Ba,Ti alkoxide precursor solutions was performed under a nitrogen atmosphere by the use of a dry box.

The alkoxide precursor solutions were hydrolyzed with $r_w = 5.0$ and 5.7, respectively. The hydrolyzed solutions were aged in a sealed container (0.5 ml in a glass bottle of 20 mm in diameter) kept still for 1 day at 0 °C, 1 day at 30 °C, elevated to 50 °C of heating rate 10 °C /day and 4 days at 50 °C, consecutively. Gelation and shrinkage of the gel network reaction took place during this period, and then wet gels dried at 90 °C for 1 day by purging oxygen gas. To investigate the microstructural changes with heat treatment, xerogels were sintered at temperatures of 500, 700, 900, and 1100 °C for 1 h in oxygen (heating rate of 10 °C/min) and then cooled in the furnace. Differential thermal analysis and thermogravimetric analysis (DTA/TG) were conducted in the temperature range from 20 to 1100 °C in oxygen (heating rate of 10 °C/min) to investigate the combustion behavior of organic compounds and weight loss in the xerogels. Densities of the samples were determined using a nitrogen adsorption porosimeter (Model Autosorb-1, Quanta-Chrome Corp., FL, USA) and/or Archimedes' method depending on the available range.

Measurements of the specific surface area, the hysteresis curve, and the pore size distribution of the xerogels and fired bodies at different temperatures were performed using a nitrogen adsorption/desorption porosimeter (Model Autosorb-1, Quanta-Chrome Corp., FL, USA). The Brunauer–Emmett–Teller (BET) method[15] was used to determine the surface area, whereas the Dollimore and Heal (DH) method[16] was used to determine the pore size distribution. Samples were degassed at 150 °C for 2 h in a helium-gas flow prior to each analysis.

The xerogels and the bodies fired at different temperatures were characterized by X-ray diffractometry (XRD) using CuKα radiation (Model M18XHF, MAC Science, JPN). The crystallite size of the samples was estimated from the diffraction peak of the (111) plane ($2\theta = 38.91°$) and the full width at half-maximum by the Scherrer equation.[17] (Instrumental broadening was calibrated by using coarse-grained Si powders as a reference.) The crystallinity of the xerogels was measured from the ratio of the X-ray intensity to the background relative to a well-crystallized, microcrystalline standard sample.[18] Additionally, change of the crystallite size and morphology in the initial and intermediate stage of sintering were investigated by transmission electron microscopy (TEM) with a Hitachi H800 at 200 kV. The microstructural developments of the xerogels as a function of sintering temperature were examined by using a field emission scanning electron microscope Hitachi S-5000H FE-SEM at 1 kV without coating.

3. Results and discussion

Transparent, partially crystallized $BaTiO_3$ monolithic xerogels obtained were platelike in shape and a few millimeters to 1 cm in size, as described in a previous paper.[14] X-ray diffraction (XRD) patterns of the xerogels and of 900 °C-fired samples are shown in Fig. 1. The xerogels contain appreciable amounts of single phase $BaTiO_3$. The average crystallite sizes calculated from X-ray line broadening of the xerogels were 7.1 and 7.9 nm for xerogels A ($r_w = 5.0$) and B ($r_w = 5.7$), respectively. The xerogels consist of an amorphous network and nano-sized pseudo-cubic $BaTiO_3$ crystallites, of which the sizes increase with increasing r_w.[19–22] The cubic phase was maintained up to 700 °C, but heat treatment at 900 °C brought about a growth of crystallites and a phase transformation to tetragonal phase. The characteristic parameters of the xerogels prepared with different r_w's are listed in Table 1.

Fig. 2 shows the comparison of the surface morphology for xerogels A and B. Xerogel A possesses a smooth surface, whereas xerogel B has a rough surface. This could be correlated with their microstructural characteristics such as porosity, particle size and the degree of agglomeration of the particles. The DT–TGA characteristics of xerogels A and B are illustrated in Fig. 3. The xerogels show a similar thermal decomposition process. Organic compounds present in the xerogels

decomposed in the temperature range of 200 to 400 °C associated with an exothermic reaction, indicated by characteristic peaks at around 260 and 350 °C. Total weight loss of xerogels A and B are 13.1 and 10.5%, respectively. The weight loss reached its maximum value at about 700 °C.

The initial (below 700 °C) and intermediate (700–900 °C) stages of sintering are investigated by nitrogen adsorption-desorption measurements. Fig. 4 shows the nitrogen adsorption-desorption isotherms for xerogels A and B sintered at 500, 700 and 900 °C. The analysis of Fig. 4(a) shows a type I characteristic.[23,24] The virtual lack of hysteresis in the desorption branch is usually interpreted by the presence of pores of smooth walls and of cylindrical shape. Fig. 4(b) illustrates a type IV isotherm, compared to the former, less volume is adsorbed at low relative pressures and a sudden increase in adsorption occurs at high pressure.[23,24] The desorption branch is also steeper. This indicates that the samples had less microporosity and a broader distribution of large pores. The steep desorption branch results from a very narrow throat size distribution. These features are consistent with the formation of necks between spherical particles.[10]

The evolution of the pore size distributions during sintering for xerogels A and B is summarized in Fig. 5, where the distribution of the logarithm of the pore size measured from the adsorption branch of the nitrogen adsorption isotherm is plotted as a function of sintering

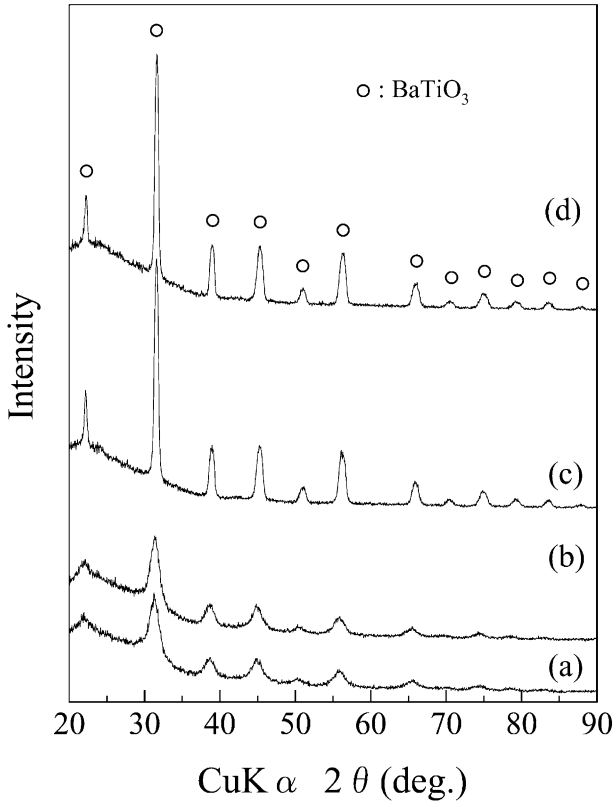

Fig. 1. X-ray diffraction patterns of the xerogels and their sintered bodies. Xerogel A; (a) as-prepared and (c) fired at 900 °C, and xerogel B; (b) as-prepared and (d) fired at 900 °C.

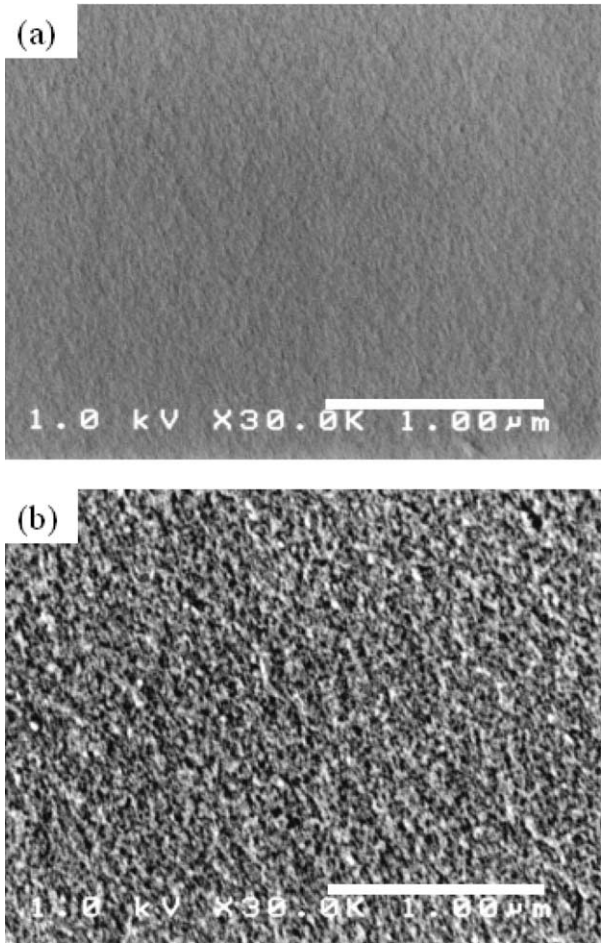

Fig. 2. FE-SEM free surface images of (a) xerogel A and (b) xerogel B, as-prepared. Bars = 1 μm.

Table 1
Specifications of the xerogels used in this study

Xerogel	Hydrolysis water content (r_w)	BET specific surface area (m^2/g)	Total pore volume, V_p (cm^3/g)	Average pore size[a] (nm)	Crystallite size (nm)	Crystallinity (%)
A	5.0	187.0	0.14	2.9	7.1	53
B	5.7	166.7	0.19	4.0	7.9	57

[a] Calculated from BET and V_p, assuming cylindrical pore geometry.

temperature. Considerable differences are observed in the pore evolution with heat treatment between xerogels A and B. Fig. 6 shows the change of the total pore volume for xerogels A and B for different sintering temperature. For xerogel A, total pore volume rapidly decreases with increasing sintering temperature. However, the total pore volume of xerogel B does not decrease until 700 °C. Fig. 7 shows changes of the grain and pore size of xerogels A and B as a function of sintering temperature. The grain size of the xerogels increases progressively with heat treatment temperature. Also, it can be seen that the pore size of the xerogels simultaneously increases until 700 °C. Above 700 °C, however, it continues to increase for xerogel B, but it decreases for xerogel A.

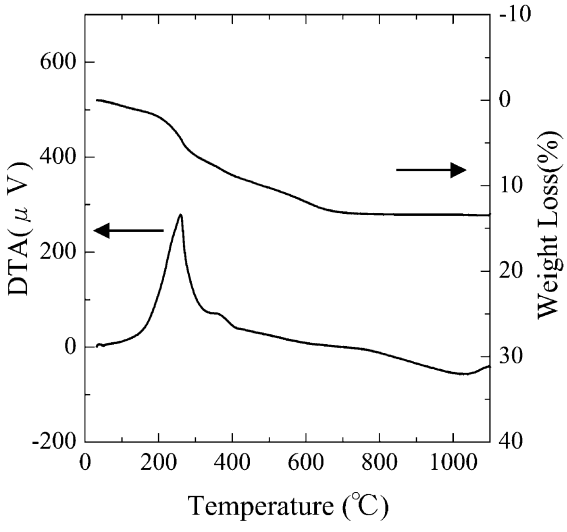

(a) Xerogel A

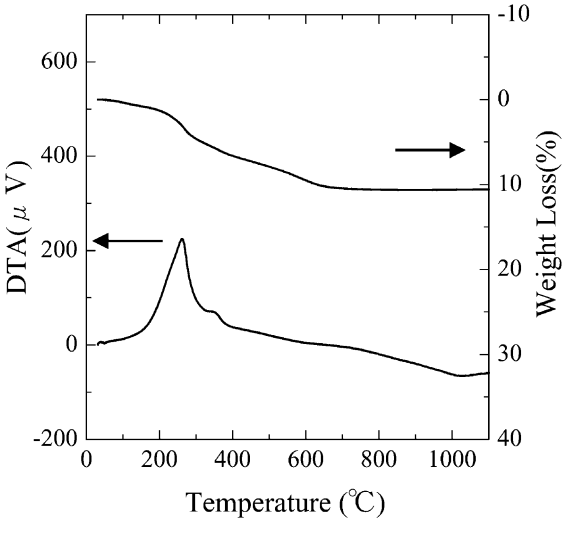

(b) Xerogel B

Fig. 3. TGA profiles for xerogels A and B.

During the initial stage of firing for xerogel A (<700 °C), small pores disappear and larger pores grow, but a drastic decrease of total pore volume is observed (Figs. 5 and 6). During the intermediate stage sintering (>700 °C), both total pore volume and average pore size decrease continuously (Figs. 6 and 7). For xerogel B, on the other hand, small pores disappear and larger pores grow in the initial and intermediate stages of sintering, resulting in a considerable increase of the average pore size from 4.0 nm in the xerogel to 15.0 nm at 500 °C, 24.2 nm at 700 °C, and 44.7 nm at 900 °C (Fig. 7). Correspondingly, the BET specific surface area (BET) decreases continuously with increasing heat treatment temperature due to pore coalescence. In addition, no change in the total pore volume, i.e., no densification, is observed below 700 °C. Above 700 °C the total pore volume decreases rapidly (Fig. 6). These significant differences seem to have a close relation with microstructural characteristics such as pore size, grain size and the degree of agglomeration. In the initial stage of heat treatment for xerogel B, small pores are eliminated presumably by surface diffusion, as it does not change the total pore volume.[25] Consequently, during this step, significant pore growth occurs. This can be explained by the concept of the equilibrium pore size above which pores do not shrink, as proposed by Kingery.[26] This concept is that a pore of a smaller size with convex faces (when observed from the outside of the pores) has to shrink, while a pore of a larger size with concave faces has to grow. Kingery and Francois[27] derived a relationship for pore stability as a function of dihedral angle and the ratio of pore size to grain size from an approximate relationship between the number of surrounding grains and the pore diameter to grain diameter ratio. The critical pore size is defined as the size of a stable pore with flat faces and can be determined if the particle size and the dihedral angle are known.[27–29] The median value of dihedral angles of 700 °C-fired samples was measured as 111° for xerogel A and 108° for xerogel B. Typical values of a dihedral angle for oxide ceramics are in the range from 100 to 150°.[26,29] Assuming an average value, the critical pore sizes of the xerogels and their sintered bodies are of the order of the grain sizes.[30] Grain size, i.e., critical pore size, and pore size of xerogels A and B are plotted as a function of sintering temperature in Fig. 7. The pore size of xerogels A and B increased until sintered at 700 °C. With increasing sintering temperature, it continued to increase for xerogel B, but it turned to decrease for xerogel A due to rapid densification. It is obvious that in the xerogel B almost all pores (average pore size is 4.0 nm) smaller than the critical pore size, assumed to be 8.0 nm, disappear after sintering at 500 °C, while those with larger diameter grow (Fig. 5). A similar tendency can be observed at higher temperature. Therefore grain size

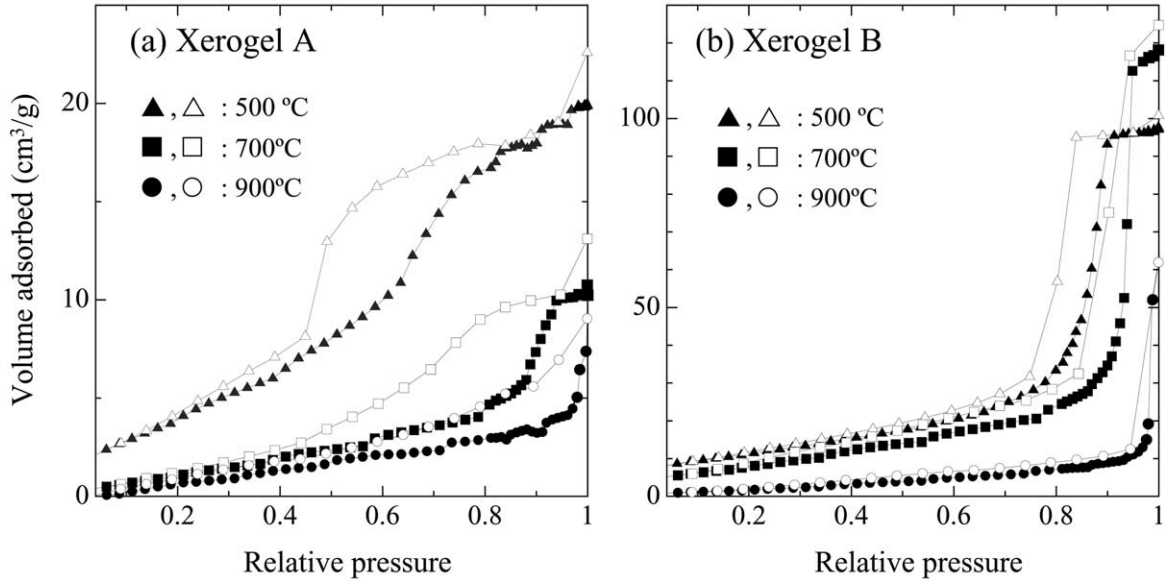

Fig. 4. Nitrogen gas adsorption-desorption isotherms obtained for xerogels A and B, heat-treated at various temperatures. (▲, ■, and ●; adsorption, △, □, and ○; desorption.)

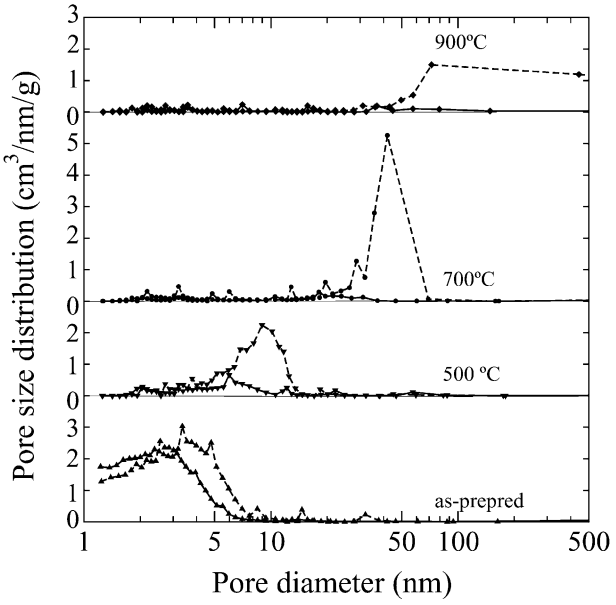

Fig. 5. Evolution of pore size distribution for xerogels A and B with increasing sintering temperature. (xerogel A;——, xerogel B;- - - -).

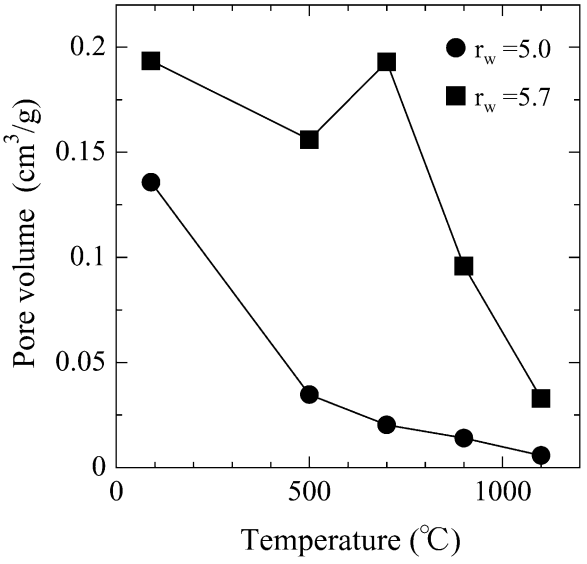

Fig. 6. Changes of the total pore volume for xerogels A and B with sintering temperature.

and pore size increase with increasing heat treatment temperature.

In the initial stage of sintering for xerogel A (<700 °C), pores smaller than the critical size disappear, similar to xerogel B, but large pores behave differently [Figs. 5 and 7(a)]. The average pore size changes from 2.9 nm in the xerogel to 7.7 nm at 500 °C, 13.8 nm at 700 °C, and 3.75 nm at 900 °C. The average pore size is smaller than the grain size at all sintering temperatures. The growth of pores larger than the critical size can be observed also, but the total pore volume is considerably smaller than in the case of xerogel B. Then, during the intermediate stage of sintering (>700 °C), the average pore size decreases again. BET surface area decreases with increasing heat treatment temperature similar to xerogel B. The total pore volume, however, exhibits quite different behavior. The enhancement of sintering for xerogel A can be explained by particle rearrangement and densification during the initial and intermediate sintering stages due to smaller pore size, lesser pore volume, and non-agglomerated crystals.[29,31,32]

Changes of the relative density of xerogels A and B as a function of heat treatment temperature are shown in

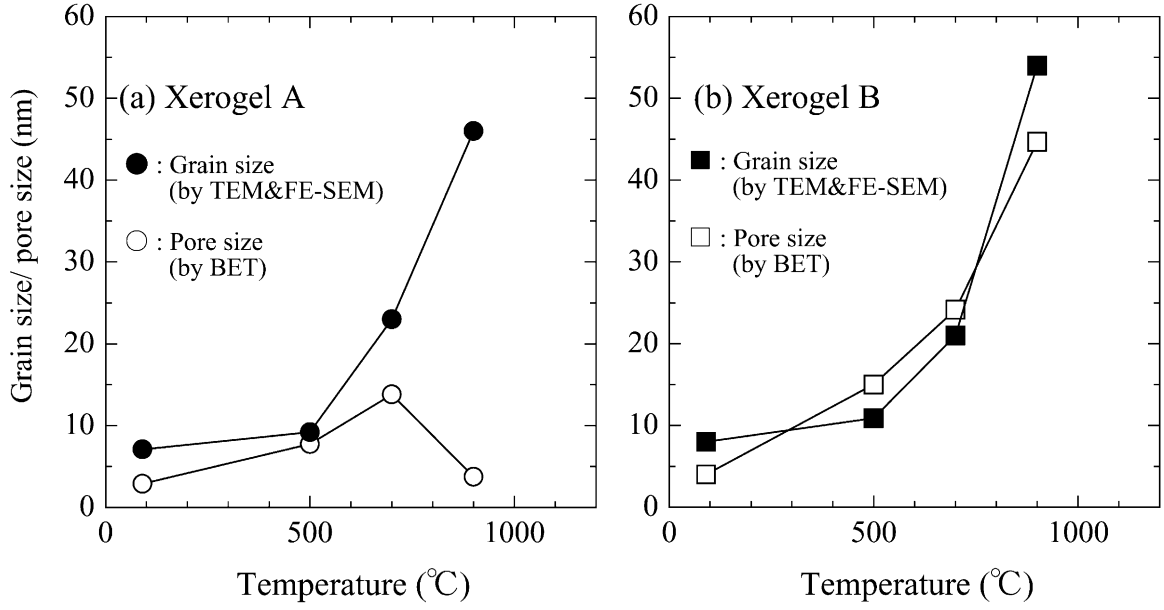

Fig. 7. Changes of the grain and pore sizes for xerogels A and B as a function of sintering temperature.

Fig. 8. The shapes of the sintering curves for xerogels A and B are fairly different. Xerogel A having smaller pore volume and pore size was sintered to a relative density of about 97% at 1100 °C. However, sintered density was only 83% for xerogel B having larger pore volume and pore size. The reason why xerogel B does not fully densify at 1100 °C, although it consists of nanometer sized grains is assumed to be as follows. During sintering, densification processes compete with coarsening processes to determine the path of microstructural evolution. If the particles in the xerogel are agglomerated, heat treatment leads to coarsening of the pore-size distribution, rather than rearrangement and densification.

Microstructural changes of xerogels A and B in the initial stage of heat treatment as a function of their internal microstructure are schematically illustrated in Fig. 9. Xerogel A having smooth and cylindrical pores with non-agglomerated crystallites shrinks during firing, accompanied by a small increase of grain size and pore size. Chen et al.[29,31] proposed a new sintering mechanism based on a model of particle repacking concurrent with particle coarsening, resulting in a higher packing factor. They assumed that particle contacts are maintained and the mass is conserved, whereas the pore space decreases and the packing factor increases. Coarsening of particles under these assumptions leads to a decrease of pore volume and an increase of packing density. As depicted in Fig. 9(a), it is considered that the high sinterability for xerogel A is attributed to particle rearrangement during particle coarsening. On the other hand, Xerogel B having pore cavities larger in diameter than the openings (throats), so-called inkbottle pores,

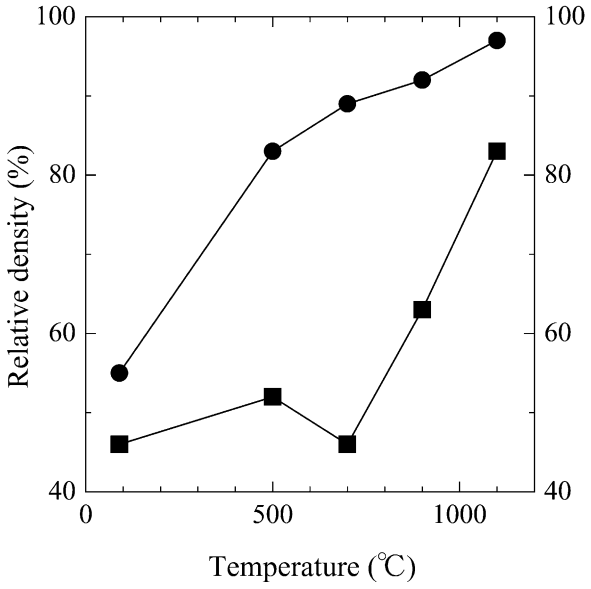

Fig. 8. Changes of the grain and pore sizes for xerogels A and B as a function of sintering temperature.

with neck-connected crystallites shrinks less, during this stage of sintering, and converts into a porous microstructure with agglomerated crystallites [Fig. 9(b)].

TEM micrographs of as-prepared, 500° and 700 °C-fired samples (initial stage of sintering) are shown in Fig. 10. The grain size of xerogel A can be seen as 7.1 (as-prepared), 9.2 (500 °C), and 23 nm (700 °C) and xerogel B as 8.0 (as-prepared), 11 (500 °C), and 21 nm (700 °C). The grain sizes measured from the TEM micrographs are in good agreement with data calculated

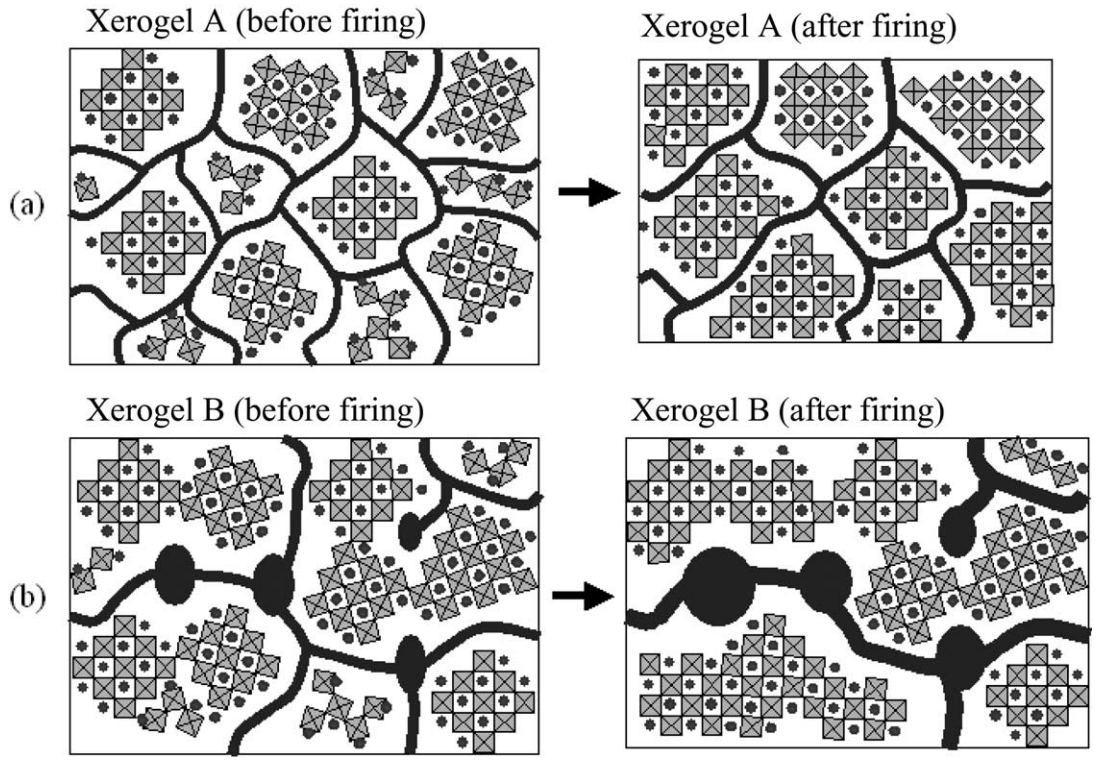

Fig. 9. Schematic illustration of the structural change of the xerogels in the initial stage of sintering, significantly affected by their internal microstructure. (●: Ba ion, and ⊠: TiO_6 octahedron.)

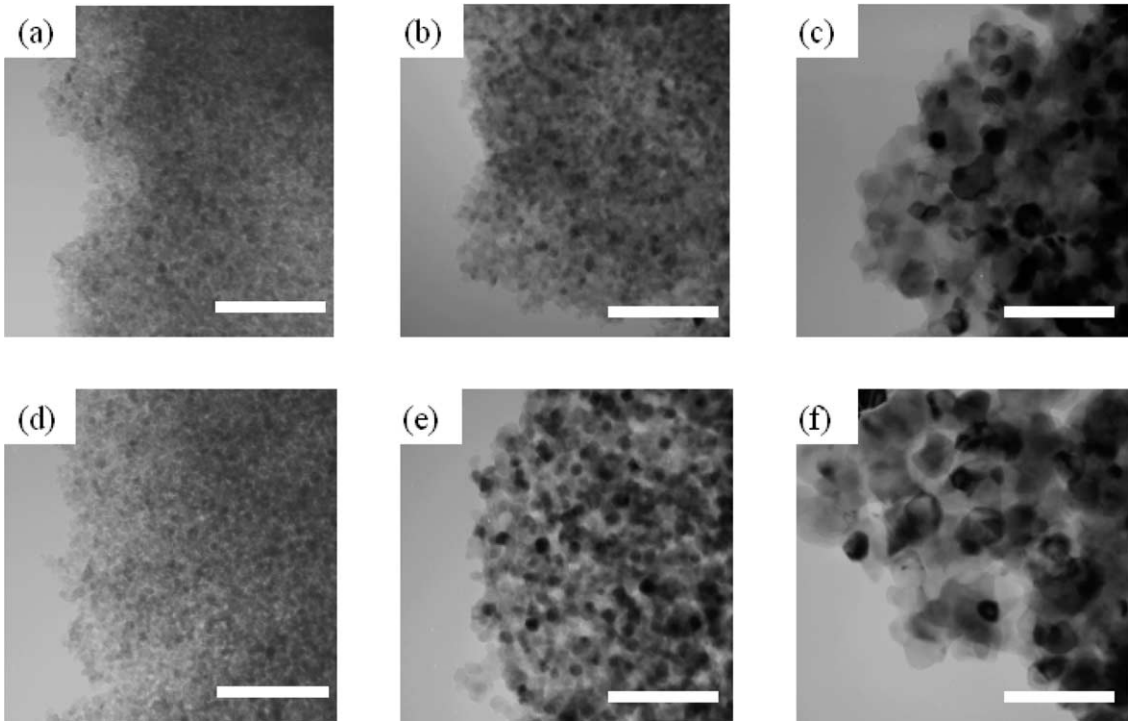

Fig. 10. TEM micrographs of the xerogels sintered at different temperatures. Xerogel A; (a) as-prepared, (b) 500 °C, and (c) 700 °C, and xerogel B; (c) as-prepared, (d) 500 °C, and (e) 700 °C. Bars = 100 nm.

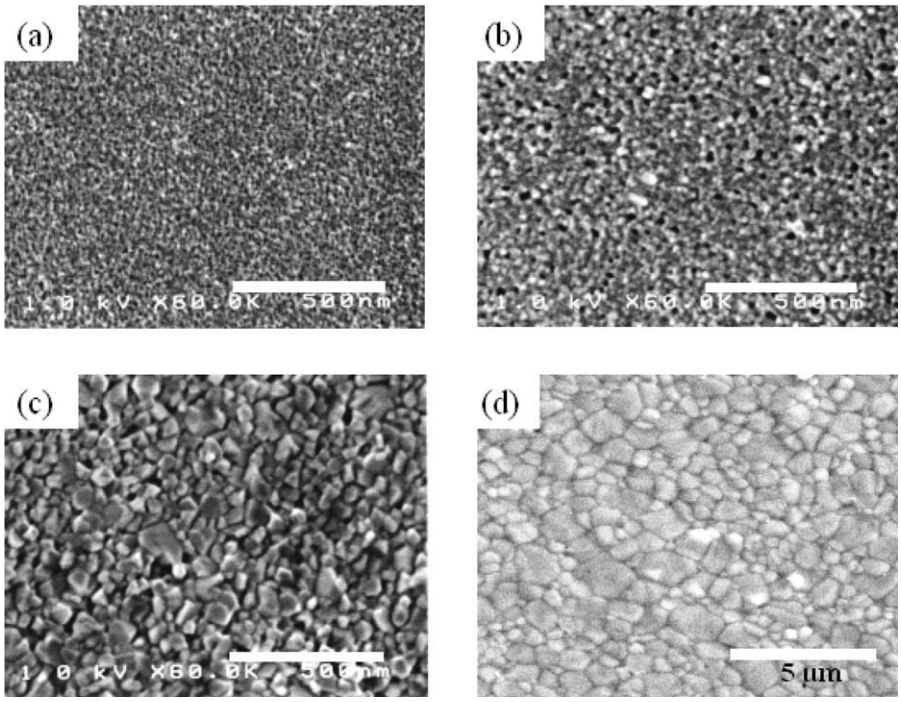

Fig. 11. FE-SEM photographs of $BaTiO_3$ ceramics from xerogel A ($r_w = 5.0$), obtained at (a) 500 °C, (b) 700 °C, (c) 900 °C, and (d) 1100 °C. Bars = 500 nm. (5 μm for (d)).

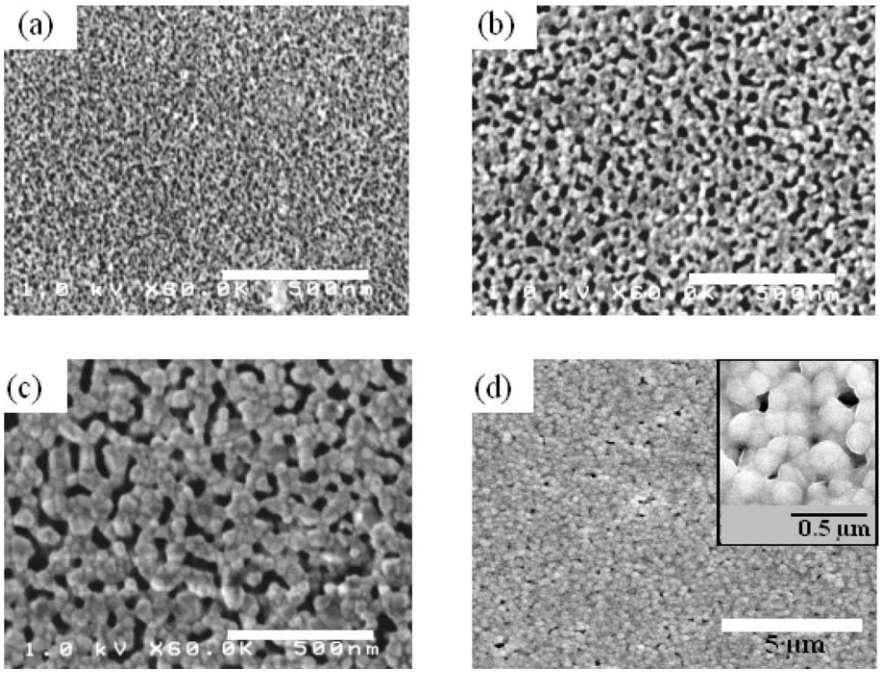

Fig. 12. FE-SEM photographs of $BaTiO_3$ ceramics from xerogel A ($r_w = 5.7$), obtained at (a) 500 °C, (b) 700 °C, (c) 900 °C, and (d) 1100 °C. Bars = 500 nm. (5 μm for (d)).

from X-ray line broadening until 500 °C. Above this temperature discrepancies are observed. Figs. 11 and 12 show the microstructural evolution of xerogels A and B with heat treatment temperature, respectively. Microstructural changes during initial and intermediate stages of sintering observed by FE-SEM match the nitrogen adsorption–desorption measurement results. $BaTiO_3$ ceramics from xerogel A sintered at 1100 °C for 1 h in oxygen converted into a dense ceramic with a grain size of about 0.5 μm. However, xerogel B converted to a porous ceramic after sintering at the same temperature. (The magnified inset illustrates the pore size difference between samples prepared from xerogel A and B.)

4. Conclusions

The microstructural evolution of xerogels prepared with different amounts of hydrolysis water ($r_w = 5.0$ and 5.7) was examined as a function of sintering temperature. The average pore size of xerogels A ($r_w = 5.0$) and B ($r_w = 5.7$) increased up to a sintering temperature of 700 °C. At higher sintering temperature, the average pore size continued to increase for xerogel B, but it decreased for xerogel A due to rapid densification. Xerogel A having smaller pore volume and pore size was sintered to a relative density of about 97% at 1100 °C. It was only 83% for the sintered xerogel B having larger pore volume and pore size. The enhancement of sintering for xerogel A having smaller pore size and pore volume, and less-agglomerated crystals can be explained by particle rearrangement and densification during the initial and intermediate sintering stages.

We can conclude from the above results that the pore size, the pore volume, and the degree of agglomeration among particles in the xerogel are important factors to fabricate dense $BaTiO_3$ ceramics at lower temperatures. It is important to note that sinterability could be additionally enhanced if xerogels with high green density can be made. High concentration sol-gel method is essential for the production of dense, pure $BaTiO_3$ ceramics directly from monolithic xerogels.

Acknowledgements

This work was supported by the Grant-in-Aid for Science Research (Grant No. 09305043) from the Ministry of Education, Science, Culture, and Sports of Japan.

References

1. Von Hippel, A. R., Dielectric materials and applications, A. R. Von Hippel, 1954, 40–45, Wiley, New York
2. Buchanan, R. C., Ceramic materials for electronics. Marcel Dekker, 1986.
3. Bruno, A. and Swanson, D. K., High-performance multilayer capacitor dielectrics from chemically prepared powders. *J. Am. Ceram. Soc.*, 1993, **76**, 1233–1241.
4. Shi, E., Cho, C. R., Jang, M. S., Jeong, S. Y. and Kim, H. J., The formation mechanism of barium titanate thin film under hydrothermal conditions. *J. Mater. Res.*, 1994, **9**, 2914–2918.
5. Cho, C. R., Shi, E., Jang, M. S., Jeong, S. Y. and Kim, S. C., Structural and electrical properties of $BaTiO_3$ thin films on Si(100) substrate by hydrothermal synthesis. *Jpn. J. Appl. Phys.*, 1994, **33**, 4984–4990.
6. Mazdiyasni, D. S., Dolloff, R. T. and Smith II, J. S., Preparation of high-purity submicron barium titanate powders. *J. Am. Ceram. Soc.*, 1969, **52**, 523–526.
7. Phule, P. P. and Risbud, S. H., Low temperature synthesis and dielectric properties of ceramics derived from amorphous barium titanate gels and crystalline powders. *Mater. Sci. Eng. B*, 1989, **B3**, 241–247.
8. Chaput, F., Boilot, J. P. and Beauger, A., Alkoxide-hydroxide route to synthesize $BaTiO_3$-based powders. *J. Am. Ceram. Soc.*, 1990, **73**, 942–948.
9. Frey, M. H. and Payne, D. A., Synthesis and processing of barium titanate ceramics from alkoxide solutions and monolithic gels. *Chem. Mater.*, 1995, **7**, 123–129.
10. Brinker, C. J. and Scherer, G. W., *Sol-Gel Science: The physics and chemistry of sol-gel processing*. Academic Press, San Diego, 1990.
11. Shimooka, H. and Kuwabara, M., Preparation of dense $BaTiO_3$ ceramics from sol-gel derived monolithic gels. *J. Am. Ceram. Soc.*, 1995, **78**, 2849–2852.
12. Shimooka, H. and Kuwabara, M., Crystallinity and stoichiometry of nano-structured sol-gel-derived $BaTiO_3$ monolithic gels. *J. Am. Ceram. Soc.*, 1996, **79**, 2983–2985.
13. Shimooka, H., Yamada, K., Takahashi, S. and Kuwabara, M., Preparation of transparent, partially-crystallized $BaTiO_3$ monolithic xerogels by sol-gel processing. *J. Sol-Gel Sci. Tech.*, 1998, **13**, 873–876.
14. Cho, J. H., Miyazawa, K. and Kuwabara, M., Influence of hydrolysis water content on the microstructure of $BaTiO_3$ xerogels prepared from high concentration metal alkoxide solutions. *J. Sol-Gel Sci. Tech.*, 2002, **23**, 9–14.
15. Brunauer, S., Emmett, P. H. and Teller, E., Adsorption of gases in multimolecular layers. *J. Am. Chem. Soc.*, 1938, **60**, 309–319.
16. Dollimore, D. and Heal, G. R., An improved method for the calculation of pore size distribution from adsorption data. *J. Appl. Chem.*, 1964, **14**, 109–114.
17. Leite, E. R., Nobre, M. A. L., Cerqueira, M. and Longo, E., Particle growth during calcination of polycation oxides synthesized by the polymeric precursors method. *J. Am. Ceram. Soc.*, 1997, **80**, 2649–2657.
18. Klein, S., Winterer, M. and Hahn, H., Reduced pressure chemical vapor synthesis of nano-crystalline silicon carbide powders. *Chem. Vap. Deposition*, 1998, **4**, 143–149.
19. Uchino, K., Sadanaga, E. and Hirose, T., Dependence of the crystal structure on particle size in barium titanate. *J. Am. Ceram. Soc.*, 1989, **72**, 1555–1558.
20. Saegusa, K., Rhine, W. E. and Bowen, H. K., Effect of composition and size of crystal phase in lead barium titanate. *J. Am. Ceram. Soc.*, 1993, **76**, 1505–1512.
21. Takeuchi, T., Tabuchi, M., Ado, K., Honjo, K., Nakamura, O., Kageyama, H., Suyama, Y., Ohtori, N. and Nagasawa, M., Grain size dependence of dielectric properties of ultrafine $BaTiO_3$ prepared by a sol-crystal method. *J. Mater. Sci.*, 1997, **32**, 4053–4060.
22. Frey, M. H. and Payne, D. A., Grain-size effect on structure and phase transformations for barium titanate. *Phy. Rev.*, 1996, **54**, 3158–3168.
23. Brunauer, S., Deming, L. S., Deming, W. S. and Teller, E., On a theory of the van der Waals adsorption of gases. *J. Am. Chem. Soc.*, 1940, **62**, 1723–1732.
24. Cohan, L. H., Hysteresis and the capillary theory of adsorption of vapors. *J. Am. Chem. Soc.*, 1944, **66**, 98–105.
25. Hahn, H., Logas, J. and Averback, R. S., Sintering characteristics of nanocrystalline TiO_2. *J. Mater. Res.*, 1990, **5**, 609–614.
26. Kingery, W. D., Bowen, H. K. and Uhlmann, D. R., *Introduction to ceramics*. Wiley, New York, 1976.
27. Kingery, W. D. and Francois, B., The sintering of crystalline oxides: I, Interactions between grain boundaries and pores. In *Sintering and Related phenomena*, ed. G. C. Kuczynski, N. A. Hooton and C. F. Gibbon. Gordon and Breach, New York, 1967, pp. 23–34.
28. Lange, F. F., Sinterability of agglomerated powders. *J. Am. Ceram. Soc.*, 1984, **67**, 83–89.
29. Chen, P. L. and Chen, I.-W., Sintering of fine oxide powders: I, Microstructural evolution. *J. Am. Ceram. Soc.*, 1996, **79**, 3129–3141.

30. Srdic, V. V., Winterer, M. and Hahn, H., Sintering behavior of nanocrystalline zirconia prepared by chemical vapor synthesis. *J. Am. Ceram. Soc.*, 2000, **83**, 729–736.
31. Chen, P. L. and Chen, I.-W., Sintering of fine oxide powders: II, Sintering mechanisms. *J. Am. Ceram. Soc.*, 1997, **80**, 637–645.
32. Chen, I.-W. and Wang, X.-H., Sintering dense nanocrystalline ceramics without final-stage grain growth. *Nature*, 2000, **404**, 168–171.